positive load, one obtains from the gravimetry and altimetry of the Maxwell Montes region a crust to a depth of 50 km with a negative density anomaly of about 500 kg m^{-3}.
26. M. T. Zuber, *J. Geophys. Res.* **92**, E541 (1987).
27. D. H. Green, *Earth Planet. Sci. Lett.* **19**, 37 (1973).
28. R. W. Carlson, *Rev. Geophys.* **32**, 337 (1994).
29. D. T. Sandwell and G. Schubert, *Science* **257**, 766 (1992).
30. G. P. Bird, *Rev. Geophys.* **33**, Suppl. (*U.S. Natl. Rep. 1991–1994*), 379 (1995).
31. P. J. Tackley, D. J. Stevenson, G. A. Glatzmaier, G. Schubert, *Nature* **361**, 699 (1993).
32. R. G. Strom, G. G. Schaber, D. D. Dawson, *J. Geophys. Res.* **99**, 10899 (1994).
33. W. M. Kaula, *Lunar Planet. Sci. Conf.* **24**, 767 (1993).
34. Both the third and the fourth moments are higher than those of a Gaussian distribution of the same mean square σ^2: >0 and $>3(\sigma^2)^2$ [W. M. Kaula, *Geophys. Res. Lett.* **20**, 2583 (1993)].
35. M. A. Ivanov and A. T. Basilevsky, *Geophys. Res. Lett.* **20**, 2579 (1993).
36. J. Arkani-Hamed, G. G. Schaber, R. G. Strom, *J. Geophys. Res.* **98**, 5309 (1993).
37. R. J. Phillips and R. E. Grimm, *Lunar Planet. Sci. Conf.* **21**, 1065 (1990); E. M. Parmentier and P. C. Hess, *Geophys. Res. Lett.* **19**, 2015 (1992).
38. R. R. Herrick, *Geology* **22**, 703 (1994).
39. J. Arkani-Hamed, *Phys. Earth Planet Inter.* **76**, 75 (1993); *J. Geophys. Res.* **99**, 2019 (1994).
40. S. C. Solomon, *Lunar Planet. Sci. Conf.* **24**, 1331 (1993).
41. D. J. Stevenson, T. Spohn, G. Schubert, *Icarus* **54**, 466 (1983).
42. A. S. Konopliv and C. M. Yoder, unpublished results.
43. C. Lithgow-Bertelloni, M. A. Richards, Y. Ricard, R. J. O'Connell, D. C. Engebretson, *Geophys. Res. Lett.* **20**, 375 (1993).
44. Currently, about 20 km^3 of crust, averaging about 6 km thick, is differentiated per year in Earth. This crust is the product of multiple differentiations extending 60 km deep, and so the volume rate of material associated with magmatism, which would release Ar, is about 200 km^3 $year^{-1}$. The volume of the mantle is 9×10^{11} km^3. Hence, if it were uniformly sampled, the entire mantle would have been cycled through the near surface layer in 4.5×10^9 years. However, convection, and hence magmatism, was much more vigorous in the past, whereas the sources of comtemporary basalts are clearly recycled. But, regardless of the numbers, the comment in the text applies.
45. This paper has been significantly improved by discussions with A. Lenardic and T. M. Harrison and by reviews by R. J. Phillips and M. T. Zuber. This work was supported in part by National Aeronautics and Space Administration grant NAGW-2085 from the Planetary Geology and Geophysics Program.

RESEARCH ARTICLE

Crystal Structure of the Ternary Complex of Phe-tRNA^{Phe}, EF-Tu, and a GTP Analog

Poul Nissen, Morten Kjeldgaard, Søren Thirup, Galina Polekhina, Ludmila Reshetnikova, Brian F. C. Clark, Jens Nyborg*

The structure of the ternary complex consisting of yeast phenylalanyl–transfer RNA (Phe-tRNA^{Phe}), *Thermus aquaticus* elongation factor Tu (EF-Tu), and the guanosine triphosphate (GTP) analog GDPNP was determined by x-ray crystallography at 2.7 angstrom resolution. The ternary complex participates in placing the amino acids in their correct order when messenger RNA is translated into a protein sequence on the ribosome. The EF-Tu–GDPNP component binds to one side of the acceptor helix of Phe-tRNA^{Phe} involving all three domains of EF-Tu. Binding sites for the phenylalanylated CCA end and the phosphorylated 5′ end are located at domain interfaces, whereas the T stem interacts with the surface of the β-barrel domain 3. The binding involves many conserved residues in EF-Tu. The overall shape of the ternary complex is similar to that of the translocation factor, EF-G–GDP, and this suggests a novel mechanism involving "molecular mimicry" in the translational apparatus.

Protein biosynthesis is a central process in every organism. It provides the link between the genetic information encoded in DNA and functional proteins. Understanding the steps of protein biosynthesis should have an impact on our overall perception of the process of translation. An essential participant in protein biosynthesis is the ternary complex of aminoacyl transfer RNA (aa-tRNA), elongation factor Tu (EF-Tu or EF-1α), and guanosine triphosphate (GTP), yet its three-dimensional structure has hitherto been unknown. The determination of this structure allows a much more precise and testable description of the molecular mechanism of protein biosynthesis.

The process of synthesizing proteins on the ribosome can be divided into initiation, elongation, and termination. Initiation and termination are punctuation events in that they deal with starting and stopping synthesis as a response to specific start and stop codons on messenger RNA (mRNA). These steps are assisted by initiation and release factors, respectively.

The central step in protein biosynthesis is elongation, in which amino acids are added one at a time to the growing polypeptide chain according to the sequence of codons present on mRNA. In prokaryotes, three elongation factors are involved as catalysts in this process: EF-Tu, the EF-Tu specific nucleotide exchange factor EF-Ts, and the translocation factor EF-G. Both EF-Tu and EF-G are members of the G protein superfamily, which consists of proteins with a conserved, common structural design (*1*). Thus EF-Tu exists in one of two states, either bound to guanosine diphosphate (GDP) as the inactive complex EF-Tu–GDP, or in the active form EF-Tu–GTP. The active EF-Tu–GTP binds aa-tRNA to form the ternary complex aa-tRNA–EF-Tu–GTP. The exposed anticodon of aa-tRNA is recognized on the ribosome by interaction with a codon on mRNA. This is part of the overall interaction between the ternary complex and the so-called A site of the ribosome. The ribosome induces hydrolysis of EF-Tu–GTP to EF-Tu–GDP, which is released from the ribosome (*2*). This inactive form of EF-Tu is recycled by the exchange of GDP for GTP, a process catalyzed by EF-Ts. The third elongation factor, EF-G, catalyzes the translocation reaction whereby the ribosome advances to the next codon on mRNA and translocates the peptidyl tRNA from the A site to the P site.

Both EF-Tu and aa-tRNA synthetases (aaRS) are proteins that can bind tRNA. However, in contrast to an aaRS, EF-Tu forms complexes with all aa-tRNAs. It is therefore expected that EF-Tu recognizes common features of all aa-tRNAs. Some structural information on how an aaRS binds to its cognate tRNA is available (*3*). A survey of features of tRNAs believed to be involved in ternary complex formation has been presented by Faulhammer and Joshi (*4*). Investigations of the specific parts or residues of aa-tRNA or EF-Tu participating in ternary complex formation have led to the formulation of possible models for the ternary complex (*5–7*). However, none of these models is in agreement with the x-ray model described in this article.

The crystal structure of yeast tRNA^{Phe} revealed the structural organization of tRNA as two double-helical segments almost perpendicular to each other (*8*, *9*). Each helical segment contains two base-

P. Nissen, M. Kjeldgaard, S. Thirup, G. Polekhina, B. F. C. Clark, and J. Nyborg are in the Department of Biostructural Chemistry, Institute of Chemistry, Aarhus University, Langelandsgade 140, DK-8000 Aarhus C, Denmark. L. Reshetnikova is at the Engelhardt Institute of Molecular Biology, Russian Academy of Sciences, 32 Vavilov str., 117984 Moscow, Russia.

*To whom correspondence should be addressed.

paired stems of the classical cloverleaf structure (Fig. 1). The acceptor helix is composed of the T stem and the acceptor stem and ends in the common 3′ CCA sequence, where the amino acid is coupled by an ester linkage to a hydroxyl group of the terminal ribose ring. The anticodon helix is composed of the D stem and the anticodon stem. The loop containing the anticodon is at the end of this helix.

EF-Tu is composed of an NH_2-terminal G domain, which binds the nucleotide cofactor, and two β-barrel domains (Fig. 1). The crystal structure of trypsin-modified EF-Tu–GDP from *Escherichia coli* is known (*10*). Crystal structures of active EF-Tu from *T. thermophilus* and *T. aquaticus* with the GTP analog GDPNP have been determined (*11, 12*). When the structures of EF-Tu–GDP and EF-Tu–GDPNP are compared, an unexpectedly large movement of domains 2 and 3 relative to domain 1 is observed. This domain rearrangement creates in EF-Tu–GDPNP a narrow cleft between domains 1 and 2, which has been predicted to bind part of the tRNA molecule (*11, 12*). *Thermus aquaticus* EF-Tu consists of 405 amino acid residues with a total molecular mass of 44.6 kilodaltons (kD).

A substantial amount of structural information on G proteins is now available. The structures of the closely related translocation factor EF-G in the GDP-bound (*13*) and in the nucleotide-free state (*14*) have been determined. Structures of the *ras* proto-oncogene product p21 and the similar proteins *Ran* and ARF are also now known (*15–18*). Structures of the much larger heterotrimeric G proteins, $G_{t\alpha}$ and $G_{i\alpha 1}$, have been reported (*19–21*).

We have already reported the purification and crystallization of the ternary complex (*22*). We now describe the results of the successful determination of the crystal structure at 2.7 Å resolution of the ternary complex of yeast Phe-tRNA^{Phe} with EF-Tu–GDPNP from *T. aquaticus*. Although the Phe-tRNA and the EF-Tu are not from the same species we believe that this structure represents a canonical model for all ternary complexes because EF-Tu–GTP has a general aa-tRNA binding capability and EF-Tu and tRNA structures are expected to be generally conserved.

Structure determination. Two data sets were collected from two different crystals at 100 K (Table 1). The structure was determined by molecular replacement with data from crystal 1 (Table 2). Models were based on the known structures of EF-Tu–GDPNP (*12*) and tRNA^{Phe} (*23*). Parts that were expected to undergo some structural alterations during complex formation were removed from the search models. Different deletion models of tRNA^{Phe} were tested, and a model with the acceptor stem and anticodon loop excluded gave the best solutions. As a control, GDPNP and Mg^{2+} were omitted from the EF-Tu model in order to see whether molecular replacement phases would reproduce electron density for the bound nucleotide. The search models for EF-Tu and tRNA represented 20 and 7.7 percent, respectively, of the total macromolecular mass of the asymmetric unit. A self-rotation function indicated pseudo three-

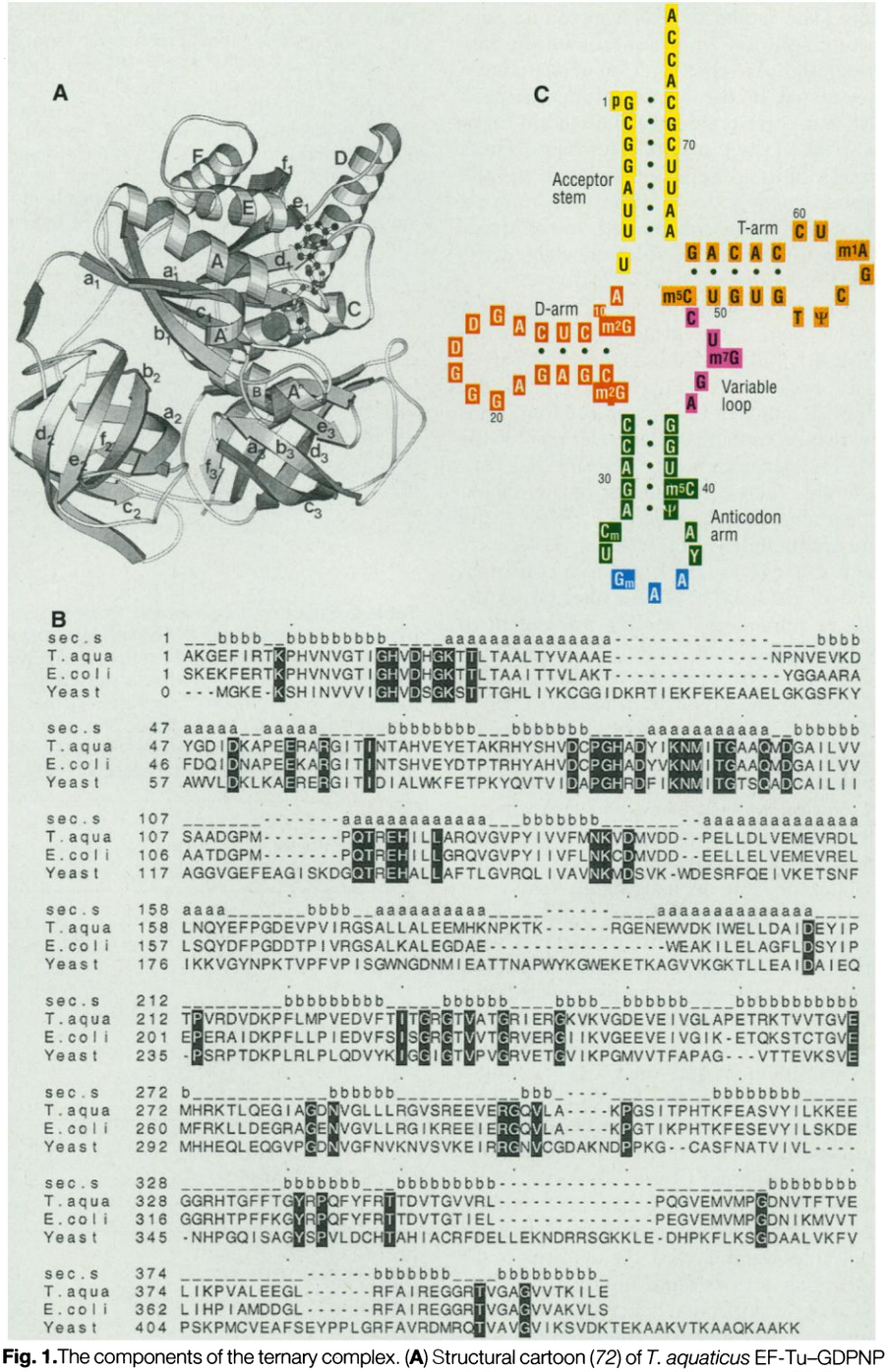

Fig. 1. The components of the ternary complex. (**A**) Structural cartoon (*72*) of *T. aquaticus* EF-Tu–GDPNP (*12*) with labels on the secondary structure elements. (**B**) Sequence alignment of *T. aquaticus* EF-Tu (*73*), *E. coli* EF-Tu (*74*), and yeast EF-1α (*75*) extracted from an alignment of the 94 complete EF-Tu and EF-1α sequences found in release 31 of the SwissProt database (*76*). Conservations observed in more than 98 percent of the sequences are shown in reverse print. The secondary structure as it appears in (A) is indicated by "sec. s." The alignment and the figure were made with the alignment editor ALMA (*77*). (**C**) The cloverleaf structure of yeast tRNA^{Phe}. The two helical segments of the tRNA structure are the acceptor helix (acceptor stem and T stem in yellow and orange) and the anticodon helix (D stem and anticodon stem in red and green). The variable loop is in violet and the anticodon is in blue.

fold symmetry, and the EF-Tu model gave three significant solutions to both the rotation and translation functions (Table 2), which were interrelated by the pseudo triad. Electron density maps were calculated on this preliminary EF-Tu structure alone, but the traces of tRNA were not interpretable. The model of tRNA gave one consistent solution when low resolution data were used. Another solution appeared as a low signal in the rotation function peak list, but corresponded to the second highest peak in the translation function. These two solutions were interrelated by the pseudo-triad, and a rotation solution for a third tRNA was constructed. In the translation function, this solution yielded the third highest peak (Table 2).

The three solutions for EF-Tu and for tRNA were refined as rigid bodies in AMORE (*24*) and subsequently as partial rigid bodies in X-PLOR (*25*) with the three domains of EF-Tu and the four stems of tRNA moving independently (Table 3). The acceptor stems were rotated considerably relative to the rest of the tRNA. Clear densities for GDPNP, Mg^{2+}, and not yet included phosphates of tRNA were seen in a $(3F_o - 2F_c)$ map as a confirmation of the model. When alternating cycles of simulated annealing refinement in X-PLOR and model building in program O (*26*) were performed, the effector loop and the CCA end could be traced in $(3F_o - 2F_c)$ maps (Table 3). Noncrystallographic symmetry (NCS) was restrained for EF-Tu molecules and tRNA molecules, and the resolution was increased to 2.8 Å. Strong densities were observed at the expected positions of the terminal adenine and phenylalanine, but an assignment could not be made with confidence. Furthermore, several parts of the anticodon helix were still badly defined in the electron density as were a few loops of the EF-Tu structure. At this stage the data from crystal 2 (Table 1) were introduced. After partial rigid body refinement and one cycle of simulated annealing with the 5.0 to 2.7 Å data, the densities for the 3′ ends became clear, and the aminoacyl group and the adenine could be assigned (Table 3).

When the anticodon helices were omitted and the NCS restraints on the tRNA molecules were released, the densities of the anticodon arm became interpretable. The NCS of the anticodon helices appeared to be imperfect and therefore the NCS restraints on the tRNA structure was split into two clusters with the three acceptor helices as one and only two of the three anticodon helices (E and F) as the other (Table 3). The simulated annealing protocol did not improve the model any further and positional refinement was continued in TNT (*27*). After one batch of TNT refinement, the map and the refinement statistics improved considerably. Subsequent cycles of refitting in O and TNT refinement with high weights on geometry and the split NCS improved the refinement statistics further.

The model includes all residues of the three Phe-tRNA–EF-Tu–GDPNP complexes and three well-defined Mg^{2+} ions found in the T stems, a total of 14,523 non-hydrogen atoms. The EF-Tu main

Table 1. Data collection. Crystallization of the purified ternary complex has been described earlier (*22*). The crystal system is monoclinic, spacegroup *C*2. For crystal 1, the unit cell parameters are a = 208.3 Å, b = 122.3 Å, c = 151.8 Å, and β = 126.7°; and for crystal 2, a = 206.8 Å, b = 122.3 Å, c = 151.6 Å, and β = 126.3°. Reflections were observed beyond 2.6 Å resolution. The ratio of mass to unit cell volume is V_m = 3.2 daltons per cubic angström. Crystals were gradually soaked into a cryoprotecting solution [20 percent (w/v) sucrose in 65 percent $(NH_4)_2SO_4$ buffer, pH 6.8] and mounted in a loop with dimensions matching the crystal. Data sets were collected at wavelength λ = 0.87 Å at 100 K with the use of an Oxford Cryostream cooling system in oscillation frames of 2.0° on a MAR image-plate at Daresbury, station 9.6. The data were processed and merged with the use of DENZO and SCALEPACK (*69*) or ROTAVATA-AGROVATA and TRUNCATE (*70*).

Data set	Resolution (Å)	Reflections (*N*)	R_{sym}* (%)	Redundancy† (*N*)	Completeness (%)	Significance‡ (%)
Crystal 1§	20.00–2.86	58,529	5.6	2.4	78.3	85.9
Crystal 1	2.91–2.86	3,024	31.3	2.4	77.5	63.8
Crystal 2‖	25.00–2.70	80,769	5.2	2.8	96.8	79.3
Crystal 2	2.79–2.70	5,417	37.6	2.4	82.7	51.6

*$R_{sym} = \Sigma|I - \langle I \rangle|/\Sigma\langle I \rangle$. †Average number of observations per reflection after rejection analysis. ‡Significance defined as percentage of observations with $I > 3\sigma$. §Processed and scaled with DENZO and SCALEPACK. ‖Processed and scaled with DENZO and ROTAVATA-AGROVATA.

Table 2. Structure determination. Rotation search and translation search. The structure was solved by molecular replacement (*24*). Normalized structure factors were calculated with ECALC (*70*). The search models used were derived from EF-Tu–GDPNP from *T. aquaticus* (*12*) (with residues 1 to 9, 43 to 64, GDPNP, and Mg^{2+} removed) and yeast $tRNA^{Phe}$ (*23*) (with nucleotides 1 to 7, 32 to 38, and 64, to 76 removed). Three solutions from the EF-Tu model and two solutions using the tRNA model were found by crossrotational and "fixed solution" translational searches. A third solution from the tRNA search model (E) was identified by a translational search based on rotational solutions generated by NCS and spanning the possible degeneration of the pseudo triad.

Search model	Fraction* (%)	Resolution (Å)	Search radius (Å)	Angles α	Angles β	Angles γ	Rank† (*N*)	Peak height‡ (%)
EF-Tu								
A	20	10.0–3.0	35	296.1	82.9	304.6	2	10.4
B				44.4	95.2	305.7	1	10.8
C				161.9	82.7	314.9	3	5.8
tRNA								
D	7.7	15.0–6.2	45	96.1	53.7	66.8	1	10.2
E				219.0	45.0	70.0		
F				335.2	57.3	56.4	85	5.7

	Resolution (Å)	Fractional coordinates x	Fractional coordinates y§	Fractional coordinates z	Rank (*N*)	Peak height‖ (%)	*R* factor¶ (%)
EF-Tu							
A	10.0–4.0	0.491	0.0	0.186	2	10.9	53.7
B		0.264	−0.308	0.199	1	13.9	52.9
C		0.245	0.234	0.122	3	8.2	54.2
tRNA							
D	15.0–5.0	0.744	0.864	0.460	1	28.2	49.2
E		0.904	0.986	0.425	3	25.8	50.0
F		0.241	0.696	0.424	2	26.2	49.5

*Percentage (in mass) of search model relative to total macromolecular content of asymmetric unit. †Rank of solution in rotation peak list. ‡Patterson correlation coefficient. §Relative y coordinates were determined by fixing solution A. ‖Patterson correlation coefficient. EF-Tu solutions alone, tRNA solutions with all three EF-Tu solutions fixed. ¶*R* factor $= \Sigma|F_o - F_c|/\Sigma F_o$, where F_o and F_c are observed and calculated structure factor amplitudes of reflections used in the translation function. *R* factors for solutions of tRNA are calculated with all three EF-Tu's fixed.

chain and most parts of tRNA, except for the D arm, appear in continuous electron density contoured at 1.25σ in all three complexes (Fig. 2).

Structure of the ternary complex. The asymmetric unit consists of three ternary complexes forming a trimer related by a pseudo-threefold axis (Fig. 3). The trimer is the basic element of the crystal lattice and the crystal contacts between trimers involve only protein-protein and RNA-RNA interactions. No protein-protein contacts are found within the trimer.

The ternary complex is elongated (115 Å by 40 Å by 64 Å) and has an overall shape resembling a corkscrew. EF-Tu and the acceptor helix form a knob-like handle and the anticodon helix forms the screw (Fig. 4). Small angle x-ray scattering studies have been performed on the complex (*28*), resulting in an overall description of the ternary complex in excellent agreement with our model. However, the results of similar experiments suggested a compact model (*29*).

All three domains of EF-Tu–GDPNP take part in the Phe-tRNA binding and interact with the CCA-Phe end and the acceptor helix on one side (Fig. 4), but only minor parts of both protein and RNA make real contacts. The binding of Phe-tRNA to EF-Tu–GDPNP can thus be described as having three main components: (i) binding of 3′ CCA-Phe (Fig. 5A), (ii) binding of the 5′ end (Fig. 5B), and (iii) binding of the T stem (Fig. 2).

The binding site for the CCA-Phe end on EF-Tu–GDPNP is formed by a narrow cleft between domains 1 and 2. The single-stranded CCA-Phe end enters this cleft below helix A″ (Figs. 4 and 5A) and docks the amino acid Phe into a pocket with the phenyl ring stacked on the side chain of His^{67}. This pocket is lined with side chains of Phe^{229}, Asp^{227}, Glu^{226}, and Thr^{239}. There is space to accommodate any of the 20 naturally ocurring amino acids. The amino ester is recognized by main chain atoms of EF-Tu. The amino group can form hydrogen bonds to the main chain CO of Asn^{285} and the main chain NH of His^{273}. The carbonyl oxygen of the amino ester can form a hydrogen bond with the main chain NH of residue Arg^{274}, the side chain of which interacts with the phosphate of A76. The ester bond is made to the 3′-OH of the terminal ribose while the 2′-OH can make a hydrogen bond with the side chain of the conserved Glu^{271}.

The electron density does not support a 2′,3′-orthoester structure, as proposed on the basis of ^{13}C-NMR (nuclear magnetic resonance) experiments on the ternary complex (*30*). Furthermore, the ester bond is 26 Å away from Arg^{59}, which fails to support the suggestion that Arg^{59} stabilizes the orthoester anion (*30*). Other ^{13}C-NMR experiments have not detected the existence of an orthoester (*31*). Residue His^{66} in *Escherichia coli* EF-Tu has been crosslinked to ε-bromo-Lys-tRNA and the same modified tRNA gave crosslinks to His^{296} of rabbit EF-1α (*7*). These residues correspond to *T. aquaticus* residues His^{67} and Arg^{274} that are both participating in the binding of the aminoacyl group (Fig. 5A).

Two protruding loops of domain 2 (*12*), which are found between the β strands a_2 and b_2 (residues 229 to 236) and d_2 and e_2 (residues 272 to 277) form a pocket for the 3′ terminal adenine. The conserved residue Glu^{271} stacks to the adenine on one side and the conserved residues Val^{237} and Ile^{231} make a hydrophobic platform for the adenine on the other side together with Leu^{289}. The phosphates at positions 74 and 75 form contacts with Lys^{52} and the three bases of A73, C74, and C75 stack in continuation of the acceptor helix and point away from the protein, which is in agreement with several observations that various substitutions of these bases do not prevent the formation of a ternary complex (*4*).

The 5′ end of the tRNA chain is bound tightly at the junction of the three EF-Tu domains (Figs. 4 and 5B). A pocket is formed by helix A″, the COOH-terminal part of helix B, and the two loops between β-strands e_2 and f_2 (residues 300 to 303), and b_3 and c_3 (residues 346 to 348). The phosphate forms a salt bridge to the conserved residue Arg^{300}, and the ribose interacts with the conserved residues Lys^{90} and

Table 3. Refinement and model building. Stages are (A) Partial rigid body refinement; (B) six alternating batches of simulated annealing and model building; (C) anisotropic *B*-factor refinement; (D) one batch of partial rigid body refinement and three cycles of simulated annealing and model building with data of crystal 2; (E) one batch of simulated annealing with anticodon helices omitted; (F) three batches of simulated annealing with split NCS and model building of anticodon helices; (G) individual *B*-factor refinement; (H) one batch of TNT refinement; (I) extensive rebuilding in O followed by six alternating batches of TNT refinement and model building. Crystallographic contacts were excluded in the NCS restraints. Simulated annealing in X-PLOR (*25*) was performed with fast or slow cooling from 1000 or 2000 K. Higher temperatures resulted in destruction rather than improvement of the tRNA structure. The parameters for the protein structure were derived by Engh and Huber (*71*), and the parameters for the tRNA structure were part of X-PLOR. TNT refinement (*27*) was performed in batches of 20 cycles of conjugate gradient refinement with *B*-factor correlation. A preliminary parameter set for tRNA, equal to the Engh and Huber set for protein, was used (*71*). The ($3F_o - 2F_c$) electron density maps were calculated in X-PLOR and TNT. The protein structure was built with the `lego` and `manip` options of O and regularly checked against a structural database with `pep_flip`. Outliers from `pep_flip` were carefully inspected. The tRNA structure was built with the manip options of O.

Stage	Resolution (Å)	Reflections* (*N*)	*R* factor (%)		
			Initial†	Final†	Free‡
A	15.0–4.0	19,741	45.9	43.0	
B	7.0–2.8	51,941	43.0	34.8	41.6
C	7.0–2.8	51,940	34.8	30.3	38.3
D	5.0–2.7	75,629	44.6	34.0	38.9
E	5.0–2.7	75,629	35.0	33.9	38.8
F	5.0–2.7	75,629	34.3	31.2	37.3
G	5.0–2.7	75,629	31.2	30.8	36.2
H	25.0–2.7	76,349	32.5	19.9	33.5
I	25.0–2.7	76,349	32.7	22.8	30.7

Scatterers	14,523
Amino acid residues	1,215
Nucleotide residues	228
Macromolecules	6
Special chemical groups	3 amino-ester bonded phenylalanines 39 modified nucleotides
Cofactors	3 GDPNP nucleotides
Ions	3 Mg^{2+} in EF-Tu, 3 Mg^{2+} in Phe-tRNA
⟨Protein B⟩ (Å^2)§	23.8
⟨RNA B⟩ (Å^2)§	31.2
Rmsd bonded atoms B (Å^2)‖	4.54
Rmsd EF-Tu NCS (Å)¶	0.19
Rmsd tRNA NCS1 (Å)#	0.16
Rmsd tRNA NCS2 (Å)**	0.29
Rmsd bonds (Å)	0.009
Rmsd angles (°)	1.60
Rmsd planar groups (°)	0.009

*Reflections with $F > 2.0\ \sigma$ after initial random removal of 5 percent of reflections for use in *R*-free calculations. †*R* factor = $\Sigma|F_o - F_c|/\Sigma F_o$ where F_o and F_c are observed and calculated structure factor amplitudes of reflections used for refinement. ‡*R* free = *R* factor of 5 percent random set of reflections removed before model refinement. §From stage G. ‖From stage I. ¶Excluding crystal contacts. #Acceptor helix cluster, excluding crystal contacts. **Anticodon helix cluster of tRNA E and F.

Asn[91]. The ribose of C2 and the phosphate of G3 are in contact with Tyr[88] and Glu[55], which interact with the conserved Arg[59]. Residue His[85] is in contact with Asp[87], which coordinates the phosphates of G3 and A64 in a regular triangle.

Two short stretches of the backbone on one side of the T stem make contacts with main and side chains exposed on domain 3 of EF-Tu (Figs. 2 and 4). Residue Arg[330] interacts with the ribose of U52 and the phosphate group of G53. The phosphate of T54 is close to His[331]. The main chain of Gly[391] makes contacts to the ribose of C63 and A64. The ribose groups of A64 and G65 interact with Gln[341] and Thr[350], respectively. The phosphate of U67 is in contact with Lys[376].

The side of the acceptor helix that interacts with EF-Tu has previously been identified by footprinting studies with analysis of RNase digestion. The positions 74, 72, 68, 64, 63, and 44 to 51 of tRNA were observed to be protected in the ternary complex (*32*) which is in good agreement with the structure (Fig. 4). The lysine residues of *E. coli* EF-Tu–GTP have been subjected to reaction with ethyl acetimidate (*33*). Three of those, Lys[2], Lys[4], and Lys[263] (corresponding to Lys[2], Lys[4], and Lys[275] in *T. aquaticus*) were reported to have a very reduced reactivity in the ternary complex. This is not in agreement with the structure where they are found in regions of EF-Tu that are not in contact with Phe-tRNA. Strikingly, the environments of these lysines are highly altered upon the conformational change in EF-Tu which take place during nucleotide exchange (*10–12*).

Structures of the components of the ternary complex. The structures of the two macromolecular components of the ternary complex are generally similar to the structures of free EF-Tu–GDPNP and tRNA^{Phe}. By alignment of all Cα atoms (*26*) of free and Phe-tRNA–bound EF-Tu–GDPNP, the greatest deviation is a 2.5 Å shift of helix A″ (residues Pro[54] to Ile[61]). Furthermore, the Cα position of Arg[274] differs by 1.9 Å. A few other differences are in the order of 1 to 2 Å and are caused by the crystal packing.

The single-stranded 3′ end of the complexed tRNA has a helical curvature induced by the binding of CCA-Phe to EF-Tu as it is observed in tRNA complexes of class II aaRS (*3*). When superimposing the T stems of the EF-Tu–bound tRNA molecules with that of free tRNA^{Phe}, some differences are observed. The tRNA in the complex exhibits a small alteration in the angle and twist between the acceptor stem and the T stem, which expands into a 16 Å shift in the position of the 3′ end. The anticodon helix is bent, though most prominently in two of the three tRNA molecules, denoted E and F (Table 2), which differ by 12 Å in the position of the anti- codon region relative to D, which again is shifted by 3 Å relative to free tRNA^{Phe}. Interestingly, tRNA molecules E and F were the most difficult to detect in the molecular replacement procedure and this explains the advantage of splitting the NCS restraints on the tRNA molecules in the model refinement. The bending is imposed by the continued stacking of the 3′-stacked anticodon onto G20 in the D loop of the neighboring tRNA in the trimer. G20 is exposed next to the conserved G19 · C56 base pair.

Discrimination in ternary complex formation. Dissociation constants for various ternary complexes are in the nanomolar range (*34*, *35*). However, affinities of individual aa-tRNAs towards EF-Tu–GTP vary within one order of magnitude (*34*). The dissociation constants of uncharged tRNA in complex with EF-Tu–GTP are several orders of magnitude higher (*36*). This large difference has been a puzzle since it is difficult to explain by the finite number of possible interactions with the amino ester group.

The binding of the T stem and the 5′ end of Phe-tRNA on the surface of EF-Tu must be independent of the presence of the aminoacyl group. A possible explanation for the specificity for aa-tRNA is that the 5′ end binding to EF-Tu and the length of the overhang of the four 3′ end

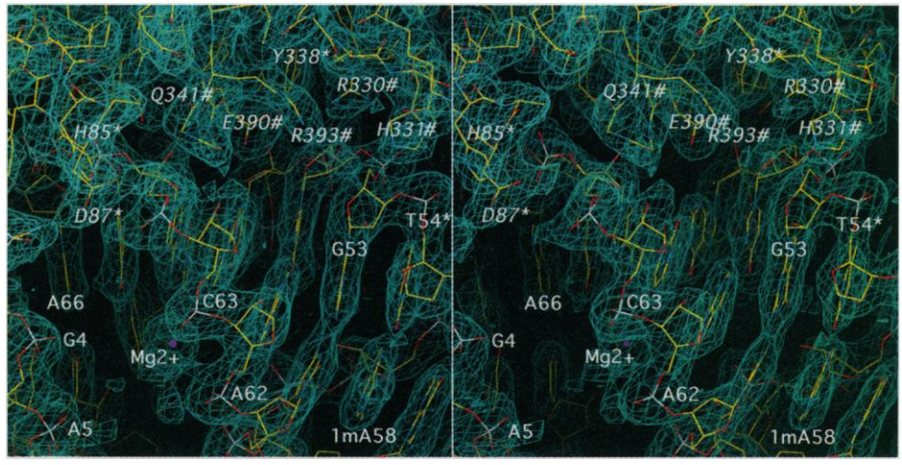

Fig. 2. Stereo diagram of the electron density of the EF-Tu–tRNA contact between domain 3 and the T stem (complex B+E). The electron density is a $(3F_o - 2F_c)$ map contoured at 1.25 σ with a cutoff radius of 2.0 Å. The Mg^{2+} ion included in the T stem of the tRNA molecules is seen. Residue labels are marked with respect to the sequence alignment, thus * represents conserved residues in all sequences and # represents conservation in prokaryotes. Amino acid labels are in italic.

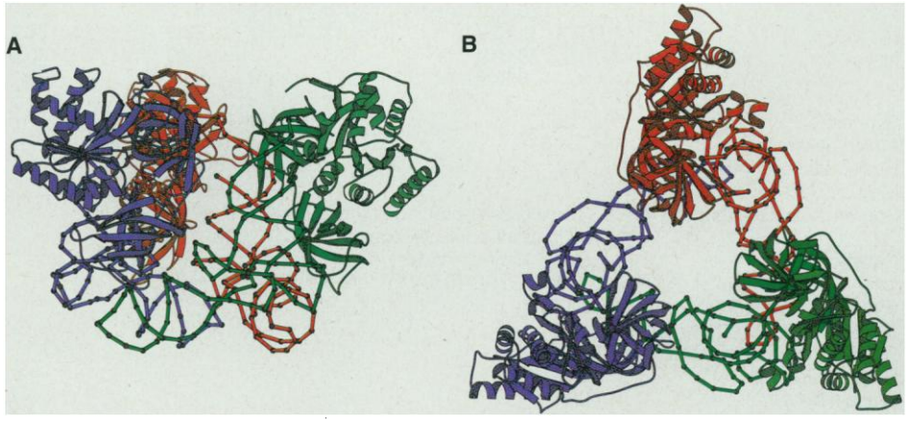

Fig. 3. Schematic representations (*72*) of the trimer forming the asymmetric unit. The EF-Tu–GTP molecules are represented as structural cartoons, and the tRNA molecules are shown as ball-and-stick connected C3′ atoms. The complexes of A+D, B+E, and C+F (table 2) are colored green, blue, and red, respectively. (**A**) Side view of the trimer, in the shape of a triangular frustum with EF-Tu flanking the top and the tRNA-tRNA contacts forming the bottom. (**B**) View along the pseudo threefold axis, with the EF-Tu molecules closest to the viewer, perpendicular to the first view. The lack of EF-Tu–EF-Tu contacts in the trimer can be seen as well as the tRNA-tRNA contacts forming corners of the trimer. See text and following figures for further detail.

nucleotides exactly allows the binding of the amino acid and the terminal adenine in their respective binding pockets between domains 1 and 2. Aminoacylation of the 3′ end regulates a "lock-and-key" match between EF-Tu–GTP and the CCA end. The additional binding energy comes from the protective binding of the amino ester, interactions with the aminoacyl side chain, and from induced interactions with the adenine and the rest of the CCA-end. The T stem and the 5′ end of uncharged tRNA can probably bind to EF-Tu–GTP, but the absence of the aminoacylation disfavors the binding of any part of the 3′ end. In prokaryotic initiator tRNA the last base pair is mismatched giving an overhang of five nucleotides. Furthermore, a formylation prevents the binding of the amino ester. Eukaryotic initiator tRNA is not formylated, but has a phosphoribosylation of nucleotide 64 which would prevent an interaction with domain 3 (*37*, *38*).

In the GDP form of EF-Tu, the tRNA binding site does not exist. Domains 2 and 3 are rotated by 90° relative to domain 1 (*11*, *12*), and the two GTPase switch regions of domain 1 adopt new conformations. Thus, all features of the aa-tRNA binding site have been moved apart. However, EF-Tu–GDP does protect the aminoacyl bond against spontaneous hydrolysis, albeit very weakly (*39*). We propose that aa-tRNA can induce an EF-Tu–GTP–like conformation of EF-Tu–GDP in an equilibrium that is shifted towards free EF-Tu–GDP and aa-tRNA.

His^{119} and aa-tRNA binding. Several studies of *E. coli* EF-Tu indicate that not only His^{66} but also His^{118} is involved in the ternary complex formation (His^{67} and His^{119} in *T. aquaticus*). Crosslinks of *trans*-diaminedichloro-platinum(II) to His^{66} and His^{118} in the ternary complex has been reported (*40*). The same two residues have been shown to be protected against photo-oxidation in the ternary complex (*41*). Finally, mutational analysis has indicated that they both participate in aa-tRNA binding (*42*, *43*). In the present structure, His^{67} interacts directly with the side chain of the aminoacyl group of Phe-tRNA. However, the structure cannot account for the apparent involvement of His^{119} in tRNA binding. This residue is buried in an interface between domains 1 and 3 in all of the structures of EF-Tu yet known, and the minimal distance to aa-tRNA is 16 Å. We suggest that part of the explanation could be the dynamic properties of EF-Tu.

When EF-Tu is transformed from the GDP form to the GTP form, or vice versa, the interface between domains 1 and 3 most likely dissociates temporarily and subsequently reassembles in the new conformation (*12*). This transformation will expose His^{119} transiently. The dynamics of this transformation must be affected by the presence of aa-tRNA that will stabilize the GTP-bound form of EF-Tu.

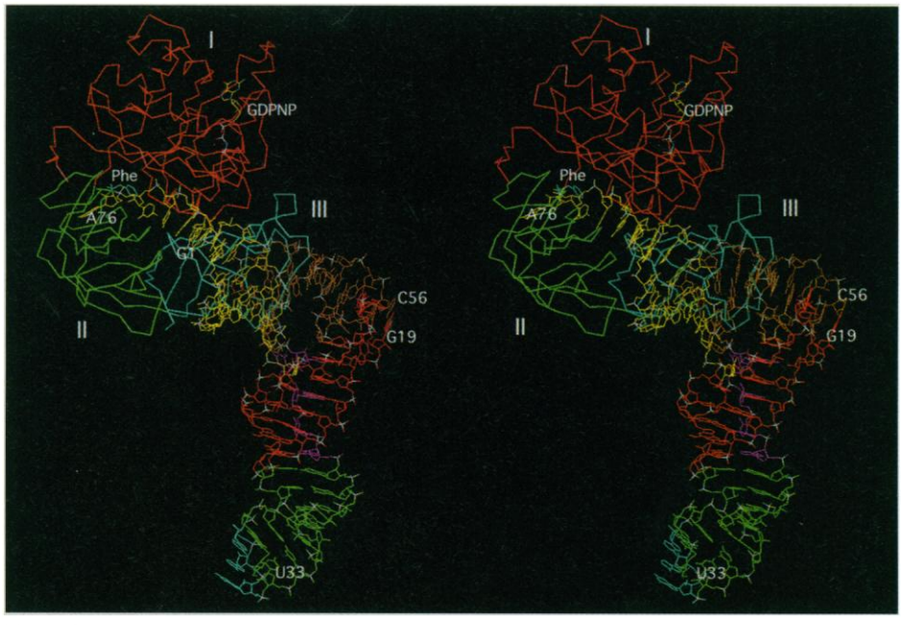

Fig. 4. Stereo diagram of the "corkscrew" structure of the ternary complex (complex C+F). EF-Tu–GDPNP is represented as a Cα trace, with domain 1 (1 to 213) in red, domain 2 (214 to 313) in green, domain 3 (314 to 405) in blue, and the GDPNP cofactor as a stick model. Phe-tRNA is colored with respect to the cloverleaf structure: acceptor stem in yellow (1 to 8 and 66 to 76), D arm in red (9 to 26), anticodon arm in green (27 to 43), variable loop in violet (44 to 48), T arm in orange (49 to 65), and the phenylalanyl group and the anticodon in blue. Phosphorus atoms are colored white.

Effector binding in G proteins. The G proteins have a common design of the G domain and a common mechanism of function has been suggested (*44*). However, the molecular design of the switch I and II regions determining the "on" and "off" state of the G proteins as a response to GDP and GTP binding may vary. This is most obvious in the response of the switch I region, which can be part of a loop in some proteins and part of a large insert in others (*1*). The response of the switch II region, where a helix changes its spatial orientation, varies in more subtle ways (*11*, *12*, *20*). The structure of the complex between Rap1A-GDPNP and a domain of an effector, c-Raf1, reveals an expected interaction between the effector and the effector loop (*45*). The functional effector of EF-Tu–GTP is aa-tRNA and the ribosome acting in cooperation. As such, the structure of the ternary complex is another example of a G protein in complex with an effector.

In EF-Tu, the switch I region is the "effector loop" between helix A and strand b_1 (residues 39 to 65) and the switch II region consists of helix B and connecting loops (residues 83 to 100). These switch regions are involved critically in the aa-tRNA binding (Figs. 4 and 5), and their conformations have not been greatly altered by the complex formation. This suggests that the switch regions of G proteins in the GTP-bound state may participate specifically in the formation of the binding site for the effector. Consequently, the switch would be unique to the target effector.

Stoichiometry of the ternary complex. We have speculated whether the quaternary structure of three ternary complexes in a trimer has a physiological role (Fig. 3). It is primarily formed through unspecific contacts. Trimers constituted of randomly selected aa-tRNAs could be advantageous with respect to the speed and fidelity of the selection process on the ribosome. The high concentration of ternary complexes in the cytosol (exceeding 100 μM) could also favor a trimeric assembly.

This is not the first proposal for a stoichiometry different from that of the classical ternary complex. A 3′-oxidized tRNA in complex with *E. coli* EF-Tu–GTP (*46*) was shown to cross-link to Lys^{208} and Lys^{237} (Lys^{219} and Lys^{248} in *T. aquaticus*), and a complex of two tRNAs per EF-Tu–GTP on the ribosome was suggested (*47*). These observations do not agree with our structure. None of these lysines is close enough to the 3′ end of tRNA to allow cross-linking without a major prior change in the conformation of the ternary complex.

A more persistent model of two EF-Tu's

per tRNA in a quinternary ("pentameric") complex (*48–50*) is based on the observation that two GTPs are hydrolyzed for each elongation cycle. Although the exact interpretation has been questioned (*51, 52*) the consumption of two GTP equivalents was also reported from studies on an XTP binding EF-Tu mutant (*53*). Two EF-Tu's are indeed in contact with one tRNA in the trimeric structure, but it seems unlikely that this could be the scaffold for a quinternary complex. However, the real question is not so much whether a quinternary complex exists as why two GTPs are consumed per peptide bond formed.

As mentioned earlier, footprinting studies identified interactions between tRNA and EF-Tu in the ternary complex monomer (*32*). Protections were observed at positions 44 to 51 and less obviously in the anticodon loop, where enhancements of nuclease digestion were also observed. This fits surprisingly well with the trimer structure, in which positions 44 to 51 are close to the anticodon loop of a neighboring tRNA and forms a corner of the trimer by the continuous stacking of the anticodon to G20. As these observations are in agreement with the RNA-RNA contacts in the trimer and originates from experiments using ternary complexes from *E. coli*, we take them as independent experimental evidence supporting our speculation that ternary complexes can exist as trimers in solution.

Comparison with elongation factor EF-G. The translocation factor EF-G exhibits a vigorous GTPase activity which is dependent on the presence of ribosomes and on the mRNA-directed binding of tRNA. In vivo, EF-G promotes fast translocation in pretranslocational ribosomes and converts them to the posttranslocational form (*54*). The crystal structures of EF-G from *T. thermophilus* in the nucleotide-free (*14*) and in the GDP form (*13*) are largely isomorphous. The molecule consists of five domains and has an overall shape resembling a tadpole, with a large head and a cylindrical tail. Domains 1 (the G domain) and 2 are structurally analogous to domains 1 and 2 of EF-Tu. Domains 3 and 5 of EF-G have topologies similar to that of the ribosomal protein S6 (*14*). Domain 4, forming the tip of the tail, reveals an unusual βαβ topology, with a left-handed crossover connection of two central β-strands. This topology is also found in the ribosomal protein S5 and in a domain of DNA gyrase (*55*).

In Fig. 6 we have aligned the Phe-tRNA–EF-Tu–GDPNP structure with EF-G, using the Cα coordinates from the G domains and the domains 2. The complete superposition of the two structures is almost perfect. Domains 3, 4, and 5 of EF-G appear to mimic the shape of the tRNA moiety of the ternary complex, with domain 3 acting as the acceptor stem, domain 5 as the T stem (and part of EF-Tu domain 3), and domain 4 as the anticodon helix. The position of the tRNA mimic of EF-G differs slightly from that of tRNA in the ternary complex. This overall resemblance of the ternary complex and EF-G represents a structural example of similarity between protein and nucleic acids counterparts. Functional mimicry of a major autoantigenic epitope of human insulin receptor by RNA has been reported (*56*) and the structure of an inhibitor of uracil-DNA glycosylase has been described as a DNA mimic (*57, 58*), which suggests that molecular mimicry is likely to be a new concept of general importance.

Translation factor interaction with the ribosome. The implication of the molecular mimicry of EF-G–GDP and the ternary complex is that they must have a common binding site on the ribosome. Most probably, this site is physically close to the ribosomal A site. This proposal is supported by the observations that both factors protect the α-sarcin loop of 23S RNA from reaction with chemical probes (*59*) and that the interaction of both factors with the ribosome is abolished if the α-sarcin loop is cleaved (*60*). In addition, the factors have been mapped on the ribosomal surface by electron microscopy with immunostaining (*61–63*), and there is a substantial correspondence between their locations.

EF-G interacts with the ribosome in its pretranslocational state, catalyzing the transition of the ribosome to its posttranslocational state (*54*). The ternary complex catalyzes the transition in the opposite direction. The overall structural similarity supports an explanation for the puzzling observation that the organization of domains 1 and 2 in the GDP form of EF-G resembles that of the GTP form of EF-Tu (*14*). Both species interact with the ribosome in its posttranslocational state.

The overall resemblance between EF-G–GDP and the ternary complex (Fig. 6) raises questions concerning the structure and function of these two elongation factors on the ribosome. Three inferences can be drawn. First, EF-G catalyzed translocation transforms the ribosome into a state with a binding pocket for a ternary complex. This pocket could be formed by the shape of EF-G–GDP after GTP hydrolysis on the ribosome. Hence, before translocation EF-G–GTP must bind to a pocket with a somewhat

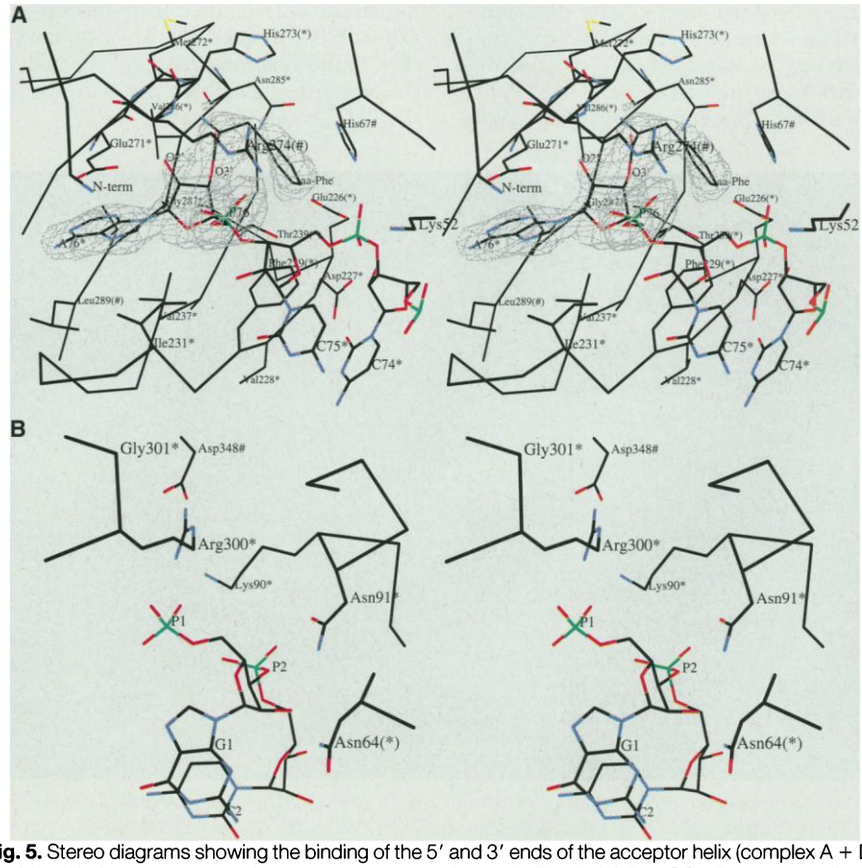

Fig. 5. Stereo diagrams showing the binding of the 5′ and 3′ ends of the acceptor helix (complex A + D). Residue labels are marked with respect to conservation as in Fig. 2. (**A**) The CCA-Phe end binding in EF-Tu–GDPNP. The electron density around the 3′ aminoacyl group has been contoured at 1.0 σ with a cutoff of 1.0 Å. (**B**) Binding of the 5′ end to EF-Tu–GDPNP.

different shape. Second, the GTPase activities of EF-G and EF-Tu must be stimulated by the same center on the ribosome. This makes it likely that all G proteins in protein biosynthesis will have their guanosine triphosphatase (GTPase) activities stimulated by this center and by the same mechanism at the same time. Third, the structural similarity suggests that the anticodon stem mimicking domain 4 of EF-G during the translocation process competes with peptidyl-tRNA for a translocation center near the codon-anticodon recognition site on the 30S subunit (*2*).

How these correlated binding pockets for EF-G and the ternary complex relate to the classical A-site on the ribosome is not clear at the moment. Nevertheless, the catalytic effect of the translation factors could be the modulation of the ribosome structure in a mechanical manner closely correlated with the GTPase induced switch of the structures of the factors.

There has been some debate on the configuration of the two tRNAs in the A and P sites on the ribosome (*64*, *65*). The two configurations, designated the R and S forms (after "Rich" and "Sundaralingam"), are based on the assumption that during peptidyl transfer the anticodons and the CCA ends must be close together. The two configurations place the A site tRNA on either side of a P site tRNA (*64*). From the present structure the binding of EF-Tu–GDPNP on one side of tRNA would exclude this side for interaction with the P site tRNA. This makes the S form the most probable configuration.

Possibility of other translation factors with tRNA-like components. It is tempting to predict some features of tRNA mimicry in the structures of the initiation and release factors. IF-2–GTP stimulates the binding of fMet-tRNA directly into the P site of the 70S (*66*), and we predict that IF-2, in analogy to EF-G, will be found to have tRNA-mimicking domains, which would occupy part of the A site during the initiation reaction and thus mediate the binding of fMet-tRNA to the P site. We find it most probable that the G domain of IF-2 is bound close to the GTPase center of the ribosome. The relative orientations of fMet-tRNA and the putative tRNA-mimicking domain of IF-2 could then provide a model for the spatial organization of the GTPase center and tRNAs in the A and P sites of the ribosome.

The release factors catalyze the final hydrolysis of the peptidyl-tRNA ester bond and the dissociation of the ribsomal subunits. In prokaryotes, three release factors, RF-1, RF-2 and RF-3, are known. Both RF-1 and RF-2 induce peptidyl-tRNA hydrolysis as a response to the stop codons on mRNA and it is further stimulated by RF-3, which is a G protein. The primary structure of RF-3 from *E. coli* shows an overall similarity with EF-G (*67*), and thus a similar structure and function can be expected. The factors RF-1 and RF-2 have been postulated to be protein analogs of tRNAs, which is very probable in light of their codon specific function and their size (*68*). Furthermore, it has long been a puzzle that a nucleic acid in the form of suppressor tRNA could compete with release factor activity. We propose that termination is a final "elongation cycle" with release factors interacting with the ribosome instead of a ternary complex and EF-G. Binding of RF-1 or RF-2 to the ribosome leads to the hydrolysis of peptidyl-tRNA. The RF-3–GTP–mediated "translocation" of RF-1 or RF-2 into the P site and of the empty tRNA into the E site results in the dissociation of the ribosome.

Following the concept of tRNA mimicry, the ancestor of all GTPases in translation must be EF-Tu which acts in conjunction with tRNA itself. In fact, this makes EF-Tu the most likely candidate for an ancestor of all G proteins since the development of a translational apparatus must have been an early event in evolution. We suggest that molecular mimicry is an important property of protein-RNA interactions involved in the process of translation and that the appearance of similarity between protein and RNA structure has been an important event in evolution.

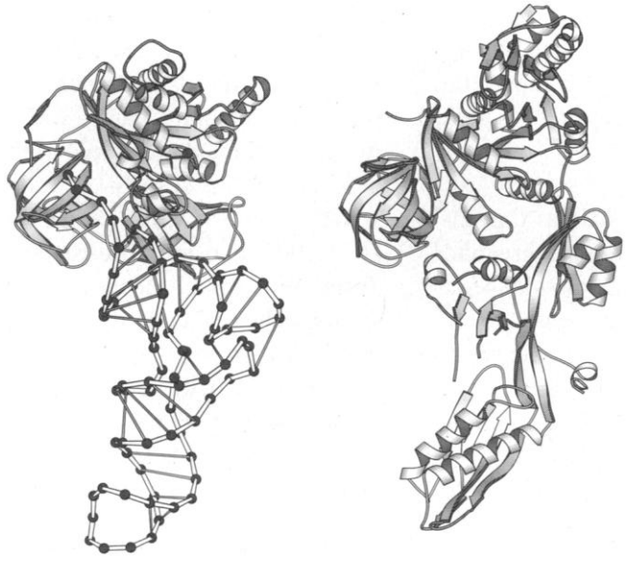

Fig. 6. Ternary complex (A+D) to the left and EF-G (*14*) to the right shown side by side in a schematic representation (*72*). EF-Tu and EF-G are shown as structural cartoons and tRNA as a ball-and-stick model of the C3′ atoms. The two molecules are shown in almost the same orientation as in Fig. 4.

REFERENCES AND NOTES

1. H. R. Bourne, D. A. Sanders, F. McCormick, *Nature* **349**, 117 (1991).
2. D. Moazed and H. F. Noller, *ibid.* **342**, 142 (1989).
3. M. Delarue and D. Moras, *BioEssays* **15**, 675 (1993).
4. H. G. Faulhammer and R. L. Joshi, *FEBS Lett.* **217**, 203 (1987).
5. C. Förster, S. Limmer, S. Ribeiro, R. Hilgenfeld, M. Sprinzl, *Biochimie* **75**, 1159 (1993).
6. B. F. C. Clark, M. Kjeldgaard, J. Barciszewski, M. Sprinzl, in *tRNA: Structure, Biosynthesis and Function*, S. Söll and U. RajBhandary, Eds. (American Society for Microbiology, Washington, DC, 1995), pp. 423–442.
7. T. G. Kinzy, J. P. Freeman, A. E. Johnson, W. C. Merrick, *J. Biol. Chem.* **267**, 1623 (1992).
8. J. D. Robertus *et al.*, *Nature* **250**, 546 (1974).
9. S.-H. Kim *et al.*, *Science* **185**, 435 (1974).
10. M. Kjeldgaard and J. Nyborg, *J. Mol. Biol.* **223**, 721 (1992).
11. H. Berchtold *et al.*, *Nature* **365**, 126 (1993).
12. M. Kjeldgaard, P. Nissen, S. Thirup, J. Nyborg, *Structure* **1**, 35 (1993).
13. J. Czworkowski, J. Wang, T. A. Steitz, P. B. Moore, *EMBO J.* **13**, 3661 (1994).
14. A. Ævarsson *et al.*, *ibid.*, p. 3669.
15. E. Pai *et al.*, *ibid.* **9**, 2351 (1990).
16. L. Tong, A. M. de Vos, M. V. Milburn, S.-H. Kim, *J. Mol. Biol.* **217**, 503 (1991).
17. K. Scheffzek, C. Klebe, K. Fritz-Wolf, W. Kabsch, A. Wittinghofer, *Nature* **374**, 378 (1995).
18. J. C. Amor, D. H. Harrison, R. A. Kahn, D. Ringe, *ibid.* **372**, 704 (1994).
19. D. G. Lambright, J. P. Noel, H. E. Hamm, P. B. Sigler, *ibid.* **369**, 621 (1994).
20. J. P. Noel, H. E. Hamm, P. B. Sigler, *ibid.* **366**, 654 (1993).
21. D. E. Coleman *et al.*, *Science* **265**, 1405 (1994).
22. P. Nissen *et al.*, *FEBS Lett.* **356**, 165 (1994).
23. A. Jack, J. E. Ladner, A. Klug, *J. Mol. Biol.* **108**, 619 (1976).
24. J. Navaza, *Acta Crystallogr.* **A50**, 157 (1994).
25. A. T. Brünger, M. Karplus, G. A. Petsko, *ibid.* **A45**, 50 (1989).
26. T. A. Jones, S. Cowan, J.-Y. Zou, M. Kjeldgaard, *ibid.* **A47**, 110 (1991).
27. D. E. Tronrud, *ibid.* **A48**, 912 (1992).
28. R. Österberg, B. Sjöberg, R. Ligaarden, P. Elias, *Eur. J. Biochem.* **117**, 155 (1981).
29. B. Antonsson, R. Leberman, B. Jacrot, G. Zaccai, *Biochemistry* **25**, 3655 (1986).
30. C. Förster, S. Limmer, W. Zeidler, M. Sprinzl, *Proc. Natl. Acad. Sci. U.S.A.* **91**, 4254 (1994).
31. J. P. Abrahams *et al.*, *Spectroscopy* **10**, 1 (1992).
32. F. P. Wikman, G. E. Siboska, H. U. Petersen, B. F. Clark, *EMBO J.* **1**, 1095 (1982).
33. B. Antonsson and R. Leberman, *Eur. J. Biochem.* **141**, 483 (1984).
34. A. Louie, N. S. Ribeiro, B. R. Reid, F. Jurnak, *J. Biol. Chem.* **259**, 5010 (1984).
35. G. Ott *et al.*, *Biochim. Biophys. Acta* **1050**, 222 (1990).
36. R. G. Shulman, C. W. Hilbers, D. L. Miller, *J. Mol. Biol.* **90**, 601 (1974).
37. S. Kiesewetter, G. Ott, M. Sprinzl, *Nucleic Acids Res.*

18, 4677 (1990).
38. R. Basavappa and P. B. Sigler, *EMBO J.* **10**, 3105 (1991).
39. A. Pingoud, W. Block, A. Wittinghofer, H. Wolf, E. Fischer, *J. Biol. Chem.* **257**, 11261 (1982).
40. M. H. Metz-Boutigue, J. Reinbolt, J. P. Ebel, C. Ehresmann, B. Ehresmann, *FEBS Lett.* **245**, 194 (1989).
41. J. Jonak, T. E. Petersen, B. Meloun, I. Rychlik, *Eur. J. Biochem.* **144**, 295 (1984).
42. J. Jonák, P. H. Anborgh, A. Parmeggianni, *FEBS Lett.* **343**, 94 (1994).
43. C. Andersen and O. Wiborg, *Eur. J. Biochem.* **220**, 739 (1994).
44. P. F. W. Stouten, C. Sander, A. Wittinghofer, A. Valencia, *FEBS Lett.* **320**, 1 (1993).
45. N. Nassar *et al.*, *Nature* **375**, 554 (1995).
46. J. M. van Noort *et al.*, *Proc. Natl. Acad. Sci. U.S.A.* **81**, 3969 (1984).
47. J. M. van Noort, B. Kraal, L. Bosch, *ibid.* **82**, 3212 (1985).
48. M. Ehrenberg, A. M. Rojas, J. Weiser, C. G. Kurland, *J. Mol. Biol.* **211**, 739 (1990).
49. J. Scoble, N. Bilgin, M. Ehrenberg, *Biochimie* **76**, 59 (1994).
50. V. Dinçbas, N. Bilgin, J. Scoble, M. Ehrenberg, *FEBS Lett.* **357**, 19 (1995).
51. M. V. Rodnina and W. Wintermeyer, *Proc. Natl. Acad. Sci. U.S.A.* **92**, 1945 (1995).
52. R. Leberman, *FEBS Lett.* **358**, 71 (1995).
53. A. Weijland and A. Parmeggiani, *Trends Biochem. Sci.* **19**, 188 (1994).
54. K. H. Nierhaus *et al.*, in *The Translational Apparatus*, K. H. Nierhaus, F. Franceschi, A. R. Subramanian, V. A. Erdmann, B. Wittmann-Liebold, Eds. (Plenum, New York, 1993), pp. 263–272.
55. A. G. Murzin, *Nature Struct. Biol.* **2**, 25 (1995).
56. J. A. Doudna, T. R. Cech, B. A. Sullenger, *Proc. Natl. Acad. Sci. U.S.A.* **92**, 2355 (1995).
57. R. Savva and L. H. Pearl, *Nature Struct. Biol.* **2**, 752 (1995).
58. C. D. Mol *et al.*, *Cell* **82**, 701 (1995).
59. D. Moazed, J. M. Robertson, H. F. Noller, *Nature* **334**, 362 (1988).
60. T.-P. Hausner, J. Atmadja, K. H. Nierhaus, *Biochimie* **69**, 911 (1987).
61. A. S. Girshovich, T. V. Kurtskhalia, T. A. Avchinnikov, V. D. Vasiliev, *FEBS Lett.* **130**, 54 (1981).
62. A. S. Girshovich, E. S. Bochkareva, V. D. Vasiliev, *ibid.* **197**, 911 (1986).
63. J. A. Langer and J. A. Lake, *J. Mol. Biol.* **187**, 617 (1986).
64. M. Yarus and D. Smith, in *tRNA: Structure, Biosynthesis, and Function*, D. Söll and U. Rajbhandary, Eds. (American Society for Microbiology, Washington, DC, 1995), pp. 443–469.
65. V. Lim *et al.*, *Nucleic Acids Res.* **20**, 2627 (1992).
66. R. Spurio *et al.*, in *The Translational Apparatus. Structure, Function, Regulation, Evolution*, K. H. Nierhaus, F. Franceschi, A. R. Subramanian, Eds. (Plenum, New York, 1993), pp. 241–252.
67. G. Grentzmann, D. Brechemier-Baey, V. Heurgué, L. Mora, R. H. Buckingham, *Proc. Natl. Acad. Sci. U.S.A.* **91**, 5848 (1994).
68. C. R. Cantor, in *Transfer RNA: Structure, Properties, and Recognition*, P. R. Schimmel, D. Söll, J. N. Abelson, Eds. (Cold Spring Harbor Laboratory, Cold Spring Harbor, NY, 1979), pp. 363–392.
69. Z. Otwinowski, Oscillation data reduction program, L. Sawyer, N. Isaacs, S. Bailey, Eds., *CCP4 Study Weekend: Data Collection and Processing* (Daresbury Laboratory, Warrington, UK, 1993).
70. CCP4 (Daresbury Laboratory, Warrington, UK, 1979).
71. R. A. Engh and R. Huber, *Acta Crystallogr.* **A47**, 392 (1991).
72. P. J. Kraulis, *J. Appl. Crystallogr.* **24**, 946 (1991).
73. R. H. Voss *et al.*, *Eur. J. Biochem.* **207**, 839 (1992).
74. M. D. Jones *et al.*, *ibid.* **108**, 507 (1980).
75. P. Cottrelle *et al.*, *J. Biol. Chem.* **260**, 3090 (1985).
76. A. Bairoch and B. Boeckmann, *Nucleic Acids Res.* **22**, 3578 (1994).
77. S. Thirup and N. E. Larsen, *Proteins* **7**, 291 (1990).
78. We thank P. B. Moore, J. Czworkowski, A. Ærsson, S. Al-Karadaghi, and A. Liljas for supplying their coordinates of EF-G, and for stimulating discussions; W. C. Merrick and J. Jonak for continued interest and fruitful discussions; L. Clowney and H. Berman for supplying updated nucleic acid geometric parameters prior to their public release, and G. Siboska and L. B. Van for technical assistance. Supported by the Protein Engineering Research Centre and the Synchrotron Radiation Committee of the Natural Science Research Council in Denmark, and by a stipend from Aarhus University (P.N.). Coordinates have been deposited in the Protein Data Bank, Brookhaven, NY, with accession number 1TTT.

11 August 1995; accepted 15 October 1995